Spatial pattern of glacier mass balance sensitivity to atmospheric forcing in High Mountain Asia – Supplementary material

Anselm Arndt, Christoph Schneider

Humboldt-Universität zu Berlin, Geography Department, 10099 Berlin, Germany
Correspondence: Anselm Arndt <anselm.arndt@geo.hu-berlin.de>

The supplementary material provides additional figures and tables referenced in the main manuscript. The information here is important for further clarification and to understand the methods in detail. Results and discussion in the study can be understood without the content of this supplementary material. This file contains the following figures and tables:

- Table S1: Applied spatial resolutions and scaling information.
- Table S2: Annual accumulated snowfall, rain, surface melt, refreezing, accumulated snowfall to total precipitation ratio, and refreezing to percolation water ratio.
- Table S3: Comparison of mean European Centre for Medium-Range Weather Forecasts Reanalysis v5-Land (ERA5-L) derived wind speed and measured wind speed at four glaciers.
- Figure S1, Figure S2, and Figure S3: Climate forcing variables.
- Figure S4: Normalised hypsometries.
- Figure S5: Annual climatic mass balance profiles of the studied glaciers.
- Figure S6: Scatterplot between Northwest/Southeast component of the glaciers and mass turnover and annual glacier-wide climatic mass balance.
- Figure S7: Uniform sensitivity characteristic. Here the reference run equals the reference run of the seasonal sensitivity characteristics.
- Figure S8 to Figure S11: Comparison of glacier-wide climatic mass balances of eight glaciers with measurements of World Glacier Monitoring Service (WGMS).
- Figure S12: Comparison of simulated and measured (WGMS) mass balance profiles of five glaciers.
- Figure S13: Comparison of glacier-wide cumulative climatic mass balances of all glaciers with two remote sensing datasets.
- Figure S14, and Figure S15: Mean monthly mass fluxes and spatial refreezing of Keli Yanghe source glacier, Naimonayi glacier, and Halji glacier.
- Figure S16, and Figure S17: Energy and mass balance terms of one glacier grid point of two glaciers on 7 July 2007.
- Figure S18: Scatterplot of mean seasonal sensitivity characteristic (SSC) and mass turnover of the 16 studied glaciers.

Table S1. Spatial resolutions (resulting glacier grid points), unscaled annual glacier-wide climatic mass balance $B_{clim,a}$, applied total precipitation *TP* scaling (to dataset of Shean and others, 2020), air temperature at 2 m T_2 offset for calculation of seasonal sensitivity characteristics, elevation at the centre of the glacier (mean e.), and model elevation of corresponding European Centre for Medium-Range Weather Forecasts (ECMWF) Re-Analysis fifth generation-Land (ECMWF) grid cell (ERA5-L e.) of Batysh Sook glacier (SOO), Zhadang glacier (ZHA), Urumqi Glacier No. 1 (UG1), Yala Glacier (YAL), Halji glacier (HAL), Bayi Ice Cap (BIC), Parlung No. 94 glacier (PL94), Keli Yanghe source glacier (KYS), Naimonayi glacier (NAI), Parlung No. 4 glacier (PL04), Chhota Shigri Glacier (CSG), Abramov glacier (ABR), Guliya Ice Cap (GIC), Muztagh Ata glaciers (MZA), Purogangri Ice Cap (PIC), and Siachen glacier (SIA).- Uncertainties of scaling factors are based on glacier mass-balance uncertainties (see Table 1 of publication) reported by Shean and others (2020).

Glacier	Resolution (GGPs) ~m (-)	Shean and others (2020) m w.e. a^{-1}	$B_{clim,a}$ raw m w.e. a^{-1}	*TP* scale -	$B_{clim,a}$ scaled m w.e. a^{-1}	T_2 offset K	$B_{clim,a}$ zero m w.e. a^{-1}	Mean e. m a.s.l.	ERA5-L e. m a.s.l.
SOO	60 (330)	0.11 ± 0.11	-1.46	1.49 ± 0.05	0.12	0.16	0.0	4156	3904
ZHA	100 (164)	−1.06 ± 0.09	-1.44	1.04 ± 0.01	-1.03	-0.31	0.01	5620	5432
UG1	100 (199)	−0.56 ± 0.22	-2.95	1.59 ± 0.06	-0.56	-0.54	0.0	3957	3714
YAL	100 (228)	−0.78 ± 0.08	-1.16	1.05 ± 0.01	-0.77	-0.26	0.0	5352	5009
HAL	100 (248)	−0.70 ± 0.08	-2.85	1.40 ± 0.01	-0.71	-0.47	0.0	5400	5154
BIC	100 (307)	−0.56 ± 0.08	-0.5	0.99 ± 0.01	-0.57	-0.57	0.0	4688	4106
PL94	100 (302)	−0.79 ± 0.08	0.71	0.69 ± 0.01	-0.79	-0.75	0.0	5299	5018
KYS	150 (191)	0.43 ± 0.07	0.53	0.91 ± 0.04	0.44	1.05	0.0	5270	4912
NAI	150 (350)	−0.36 ± 0.04	-0.64	1.07 ± 0.02	-0.35	-0.57	0.0	6030	5376
PL04	200 (321)	−0.56 ± 0.06	1.19	0.48 ± 0.01	-0.54	-1.32	0.0	5379	4789
CSG	300 (209)	−0.48 ± 0.05	-0.65	1.06 ± 0.02	-0.48	-0.99	0.0	5011	4843
ABR	300 (291)	−0.26 ± 0.04	-0.8	1.15 ± 0.01	-0.27	-0.49	0.0	4163	3968
GIC	800 (199)	−0.37 ± 0.03	0.28	0.61 ± 0.02	-0.38	-0.92	0.0	5978	5832
MZA	1000 (353)	0.21 ± 0.17	-0.14	1.23 ± 0.20	0.21	1.07	0.0	5316	5144
PIC	1200 (312)	−0.34 ± 0.25	-1.49	1.31 ± 0.08	-0.36	-0.36	0.01	5805	5756
SIA	1500 (554)	−0.02 ± 0.03	0.36	0.78 ± 0.01	-0.01	-0.11	0.0	5502	5401

Table S2. Annual (mass-balance years 2001-2018) accumulated snowfall SF_c, rain, surface melt, refreezing, ratio SF_c to total precipitation *TP*, and ratio of refreezing (Ratio refreez.) to percolation water (surface melt + rain + subsurface melt + condensation). Full glacier names are provided in the caption of Tab. S1.

Glacier	SF_c m w.e. a^{-1}	Rain m w.e. a^{-1}	Surface melt m w.e. a^{-1}	Refreezing m w.e. a^{-1}	Ratio SF_c/TP %	Ratio refreez. %
SOO	0.51	0.34	1.23	0.95	60	58
ZHA	0.44	0.45	2.07	0.85	50	33
UG1	0.46	0.52	1.79	0.88	47	37
YAL	1.12	0.95	2.83	1.13	54	29
HAL	0.63	0.42	1.91	0.73	60	30
BIC	0.42	0.31	1.8	0.94	57	43
PL94	0.67	0.22	2.09	0.79	76	32
KYS	0.47	0.09	0.44	0.47	84	85
NAI	0.43	0.13	1.36	0.8	77	51
PL04	0.73	0.13	1.98	0.86	85	38
CSG	0.89	0.19	2.14	0.92	83	38
ABR	0.69	0.39	1.85	1.02	64	43
GIC	0.22	0.03	0.69	0.26	88	35
MZA	0.43	0.07	0.55	0.4	86	63
PIC	0.48	0.32	1.29	0.67	60	41
SIA	0.45	0.01	1.01	0.62	98	59

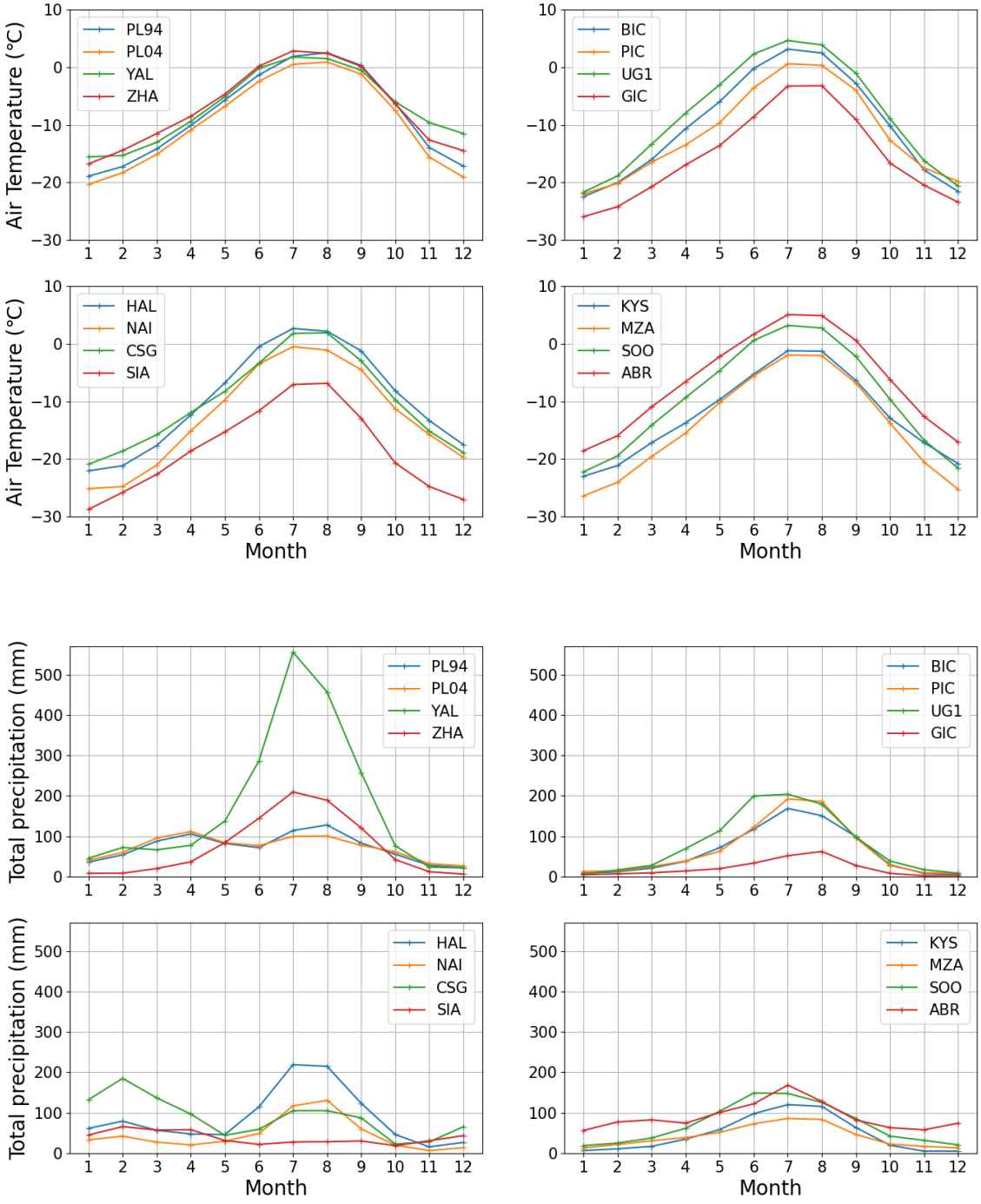

Fig. S1. Long-term (2001–2018) mean annual cycles of air temperature at 2 m and total precipitation (mm month^{-1}). The values are bias-corrected data at the mean elevation of each glacier. Full glacier names are provided in the caption of Tab. S1.

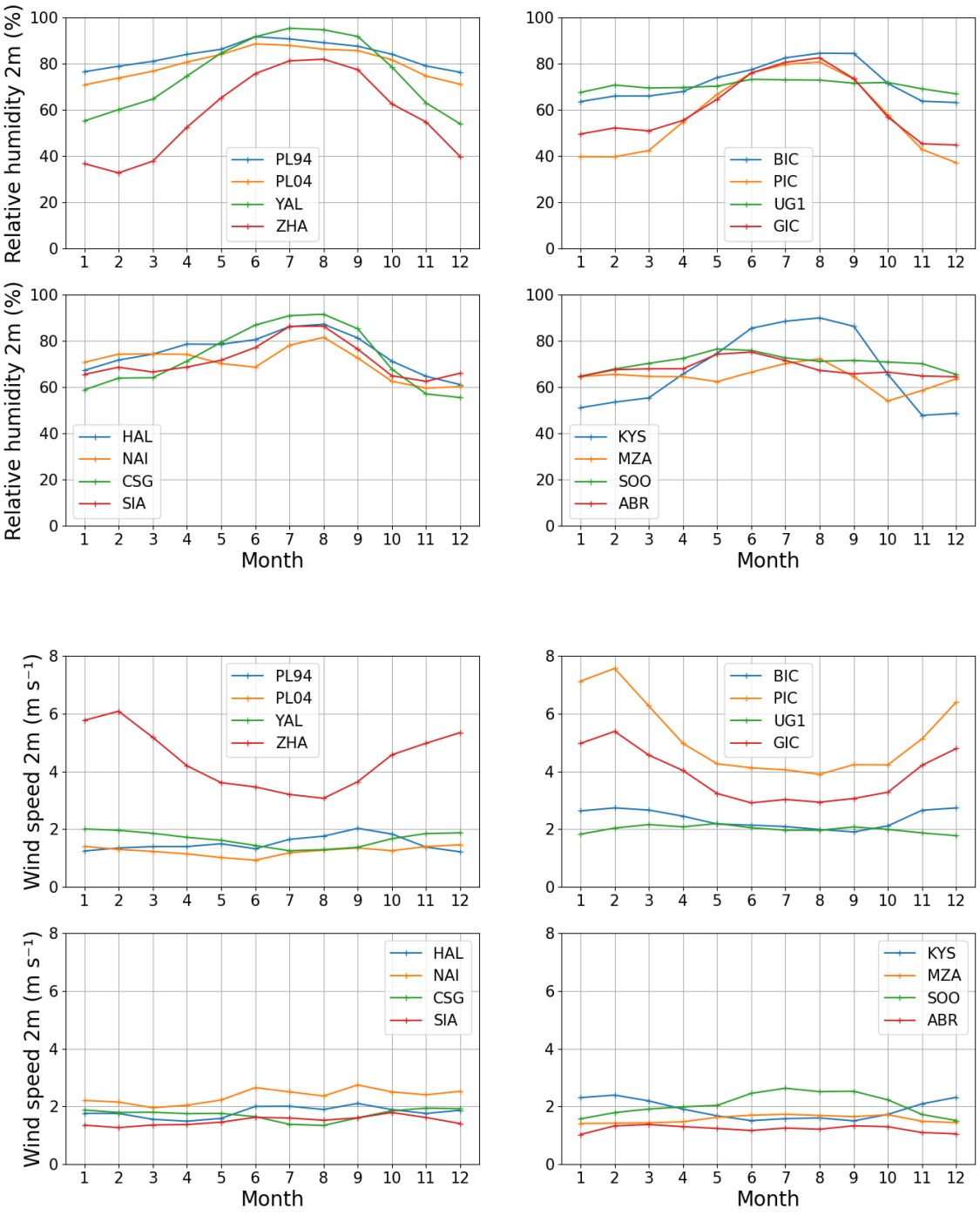

Fig. S2. Long-term (2001–2018) mean annual cycles of relative humidity at 2 m and wind speed at 2 m. The values are bias-corrected data at the mean elevation of each glacier. Full glacier names are provided in the caption of Tab. S1.

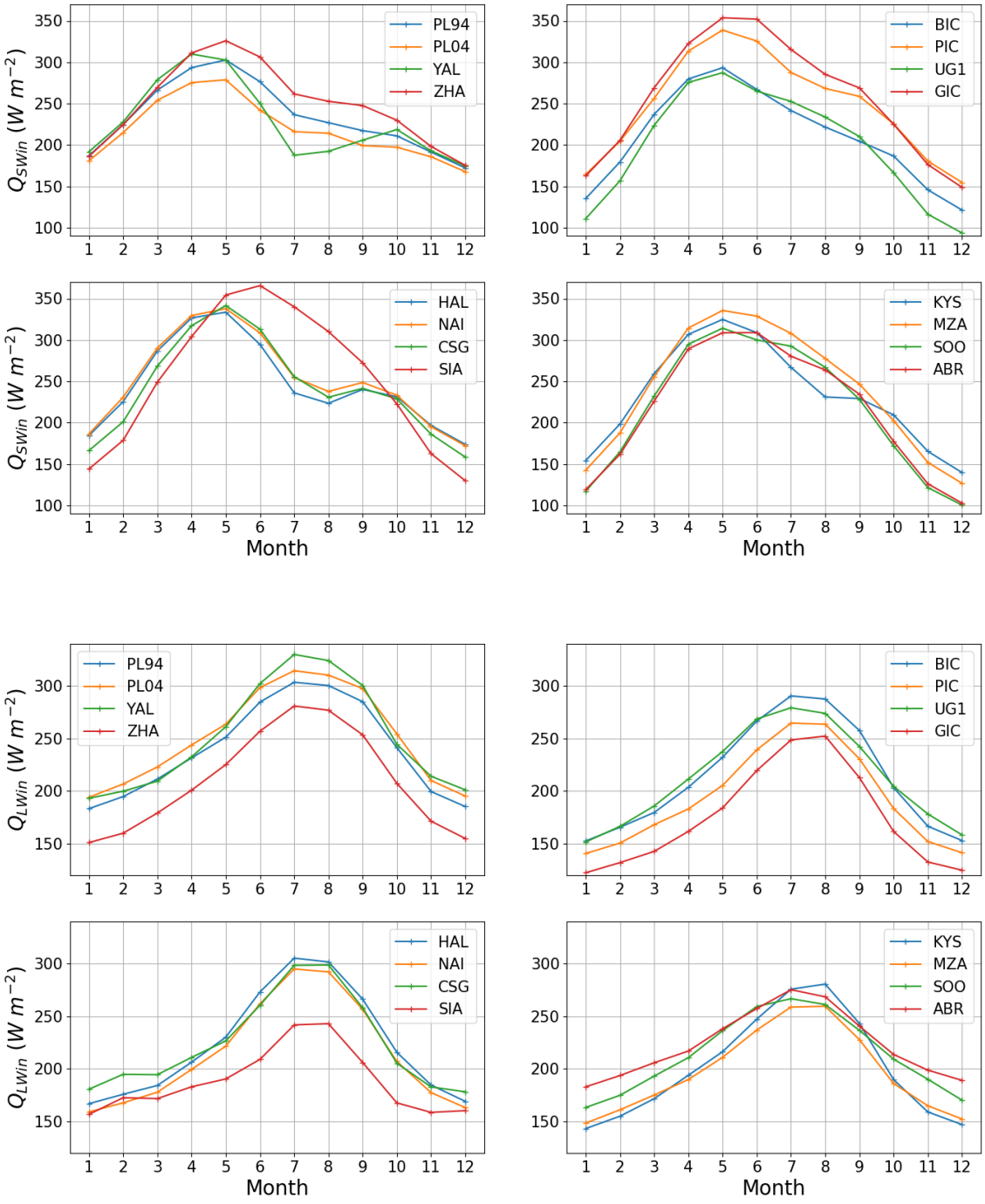

Fig. S3. Long-term (2001–2018) mean annual cycles of incoming shortwave radiation Q_{SWin} and incoming longwave radiation Q_{LWin}. The values are bias-corrected data at the mean elevation of each glacier. Full glacier names are provided in the caption of Tab. S1.

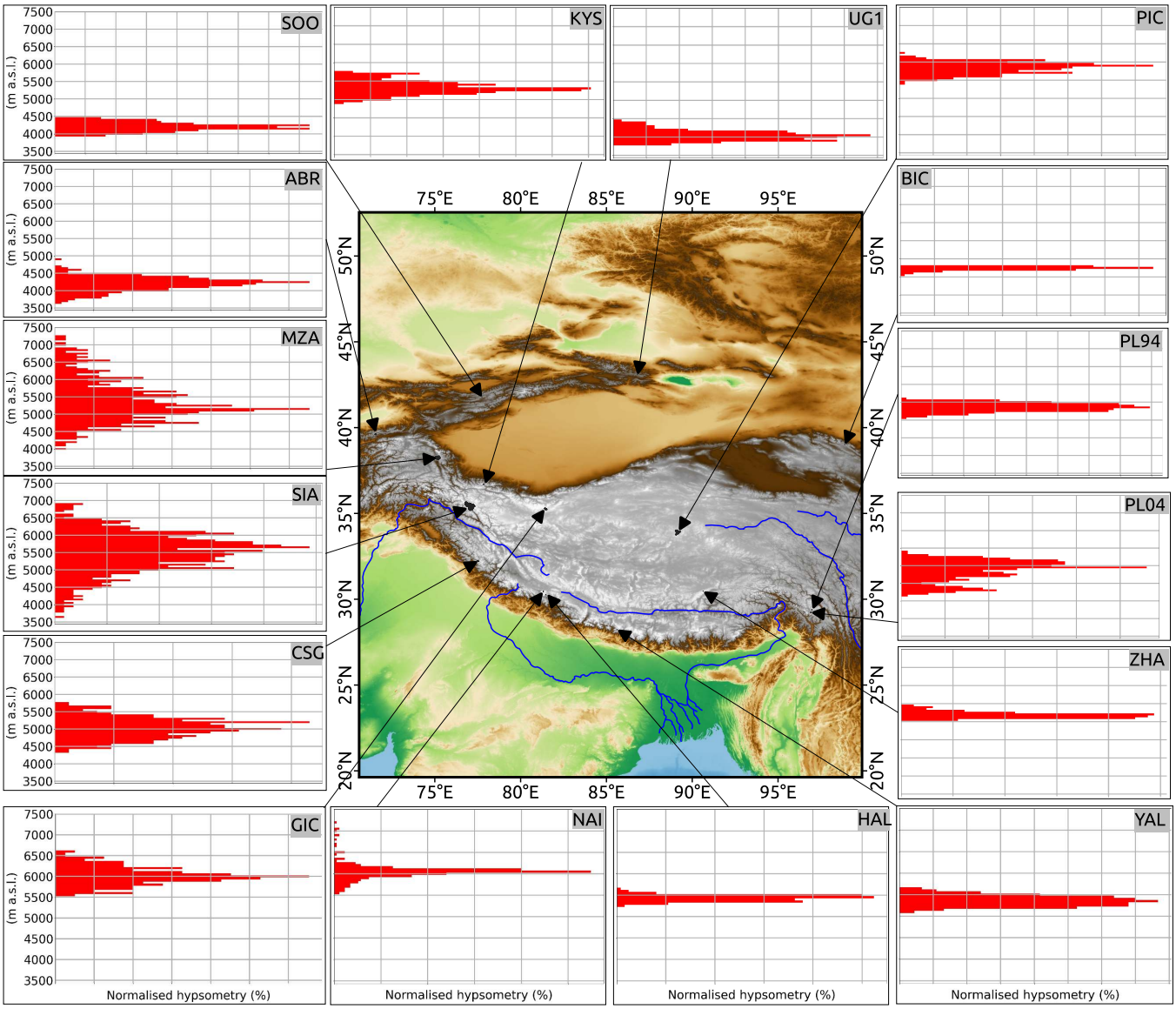

Fig. S4. Normalised not area-weighted hypsometries (50 m bands). Glacier area per 50 m band is displayed as percentage of total glacier area. Full glacier names are provided in the caption of Tab. S1.

Table S3. Comparison of mean ERA5-L derived wind speed at 2 m U_2 ($m\,s^{-1}$) with mean measured U_2 at Parlung No. 94 glacier (PL94), Zhadang glacier (ZHA), Chhota Shigri Glacier (CSG), and Yala Glacier (YAL) reported by different studies. *The U_2 YAL value is according to Fig. 5 in Stigter and others (2018) slightly below ($2\,m\,s^{-1}$) between October and April.

Glacier (study compared with)	ERA5-L derived value	Value of study
PL94 (Zhu and others, 2018)	1.5	3.2
ZHA (Zhu and others, 2018)	4.4	3.5
CSG (Azam and others, 2016)	1.7	4.1
YAL (Stigter and others, 2018)	1.7	slightly below 3*

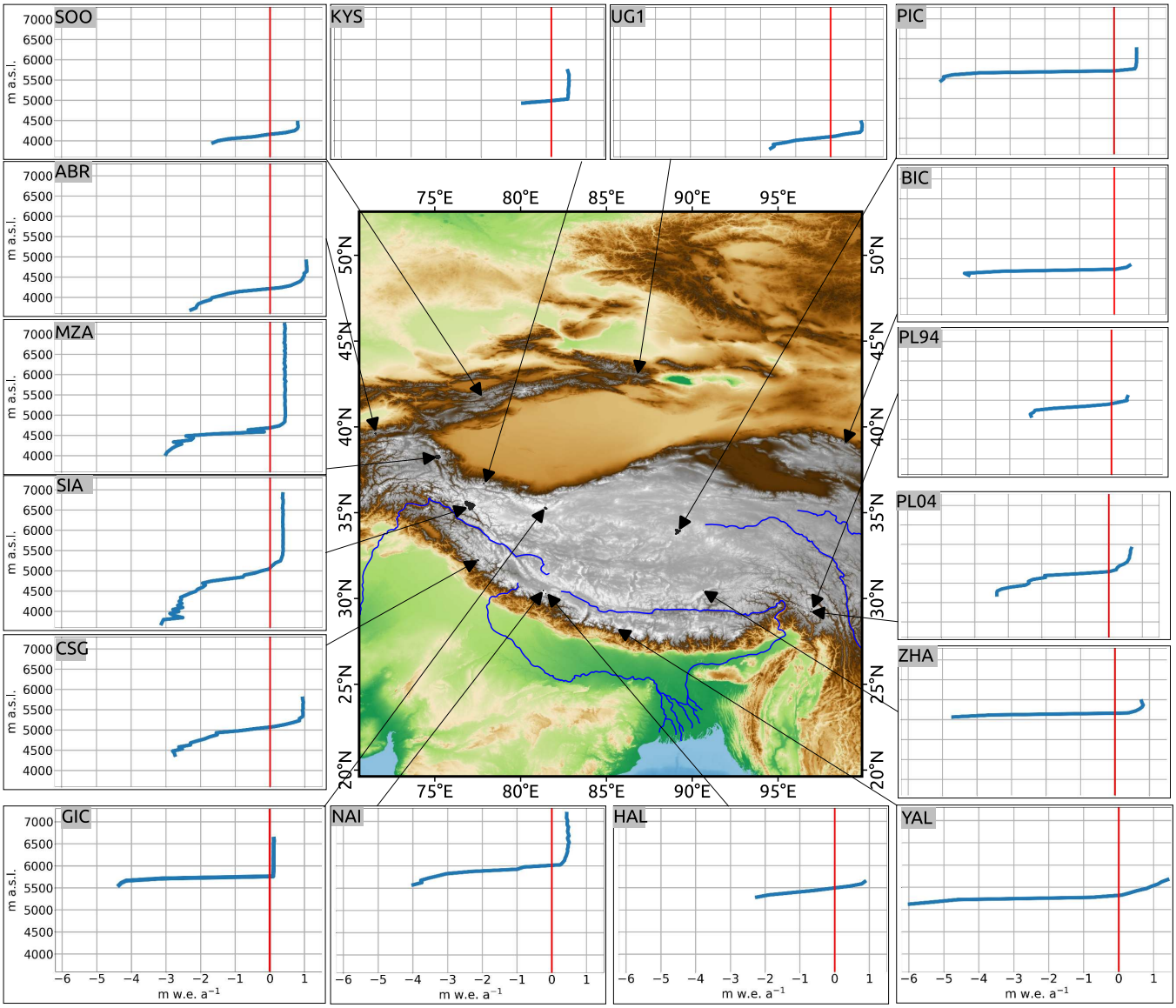

Fig. S5. Annual climatic mass balance profiles (mean mass-balance years 2001-2018) in 50 m bands. For each 50 m band the mean value of the climatic mass balances is displayed. Full glacier names are provided in the caption of Tab. S1.

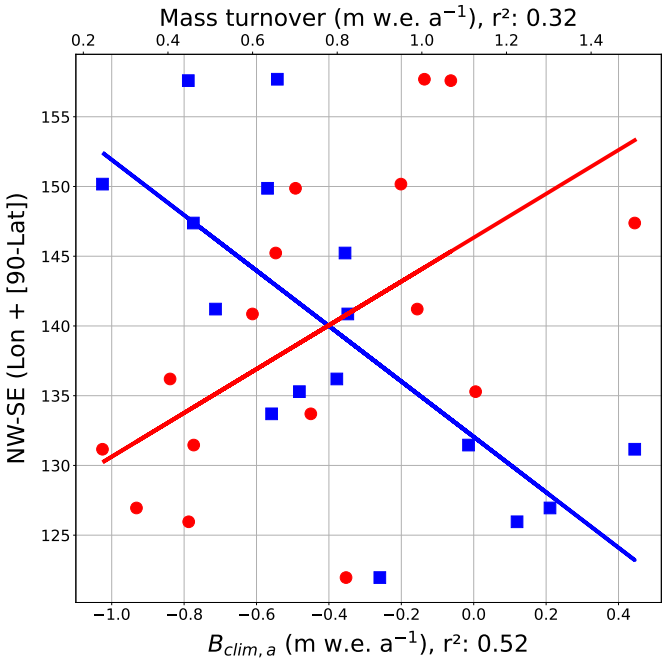

Fig. S6. Scatterplot of Northwest/Southeast location of the glaciers and mean annual glacier-wide climatic mass balance $B_{clim,a}$ (blue) and mass turnover (red) of all 16 glaciers (mass-balance years 2001-2018). Correlations are statistically significant ($p < 0.01$). A linear least-square regression model is used for the statistics. Coloured lines are the resulting regression functions.

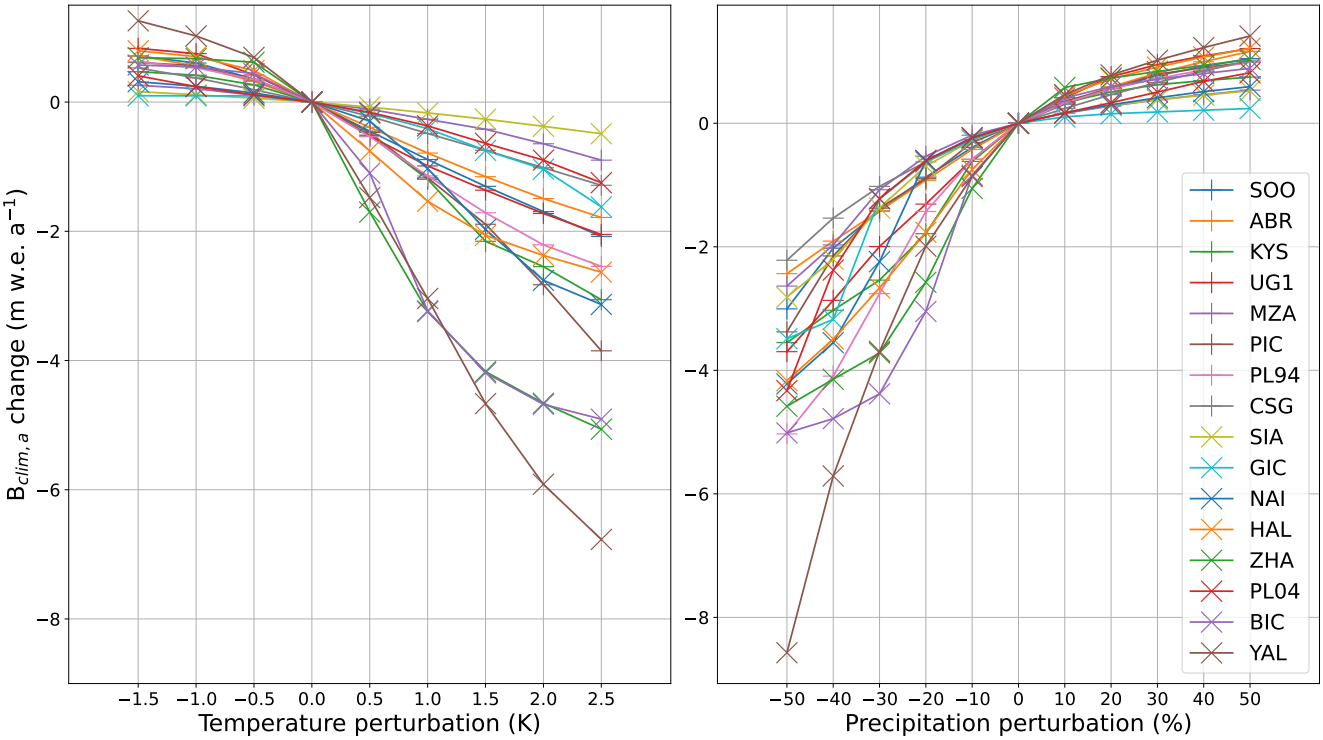

Fig. S7. Uniform sensitivity characteristics. Displayed are the annual glacier-wide climatic mass balance $B_{clim,a}$ changes to the simulations without perturbations. Other than in Fig. 7 in the publication, here the reference simulation is the reference simulation of the seasonal sensitivity characteristics (glacier-wide cumulative climatic mass balance over the whole study period in equilibrium, cf. Oerlemans and Reichert, 2000). Note the different scaling of the y-axes in comparison with Fig. 7 in the publication. Full glacier names are provided in the caption of Tab. S1.

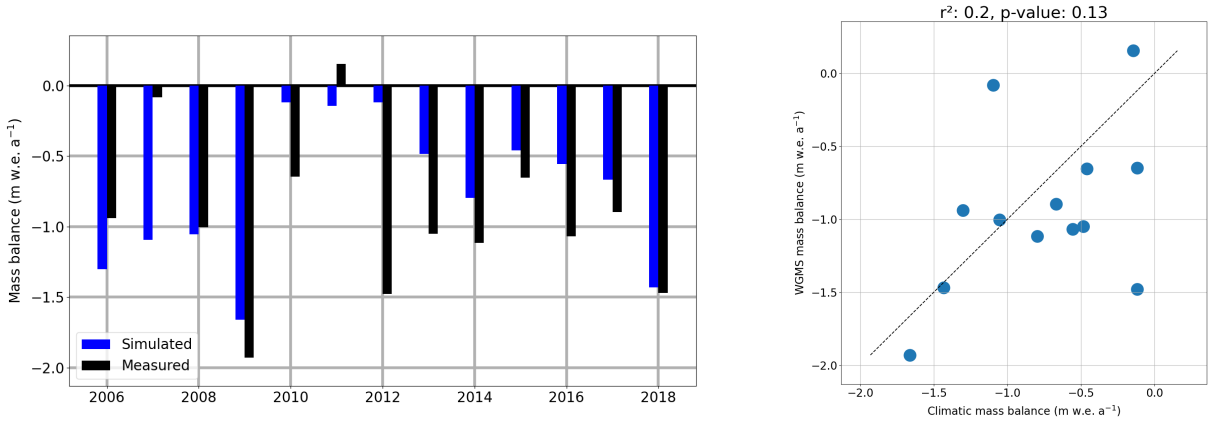

Fig. S8. Comparison of annual glacier-wide climatic mass balance of Parlung No. 94 glacier with mass balance measurements published by the World Glacier Monitoring Service (WGMS, 2021).

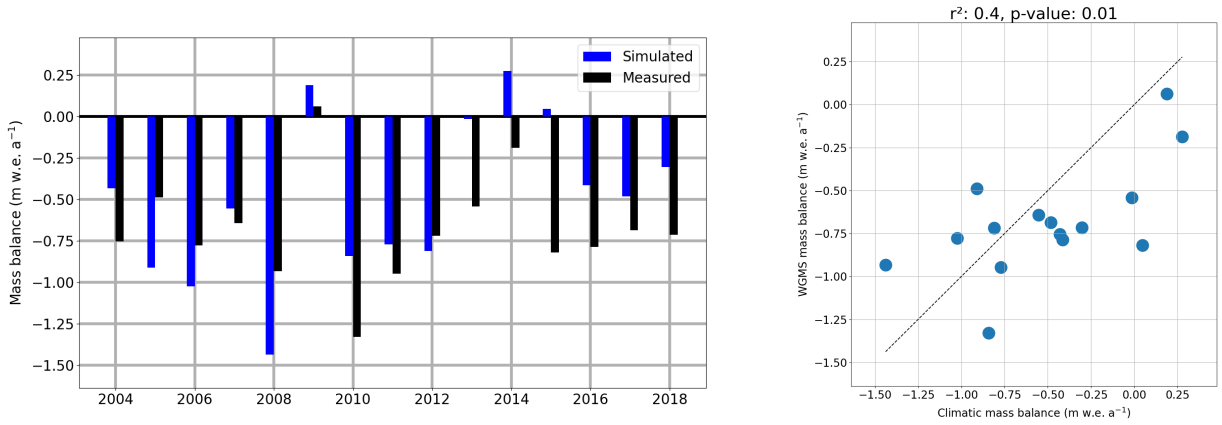

Fig. S9. Comparison of annual glacier-wide climatic mass balance of Urumqi Glacier No. 1 with mass balance measurements published by the World Glacier Monitoring Service (WGMS, 2021).

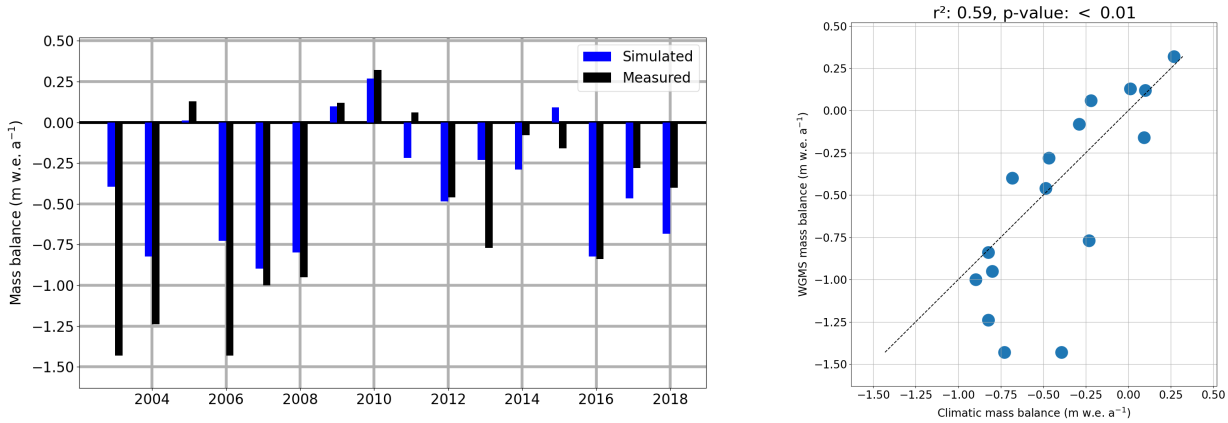

Fig. S10. Comparison of annual glacier-wide climatic mass balance of Chhota Shigri Glacier with mass balance measurements published by the World Glacier Monitoring Service (WGMS, 2021).

The comparison between simulated $B_{clim,a}$ and measured mass balances data of the World Glacier Monitoring Service (WGMS, 2021) for glaciers with short time series (< 9 mass-balance years) is displayed in Fig. S11. No statistical assessment is meaningful due to the small sampling size in the case of those five glaciers. In the case of YAL and PL04, the general pattern of the measured interannual mass balance variability is captured by the simulated $B_{clim,a}$, whereby in the case of PL04 only two years of measurement exist. The estimated geodetic estimate of SOO is positive in the Shean and others (2020) dataset. Therefore, the simulated mass balances are positive as well. Since WGMS reports a negative mass balance in all years, no agreement between simulations and the WGMS dataset can be obtained.

The measured mass balance of ABR and NAI cannot be reproduced by the simulated $B_{clim,a}$. Within the framework of this study, we cannot work out reasons for this. Kronenberg and others (2022) report a mean bias of 0.28 m w.e. a^{-1} for ABR for the period 2012-2020 compared with 0.43 m w.e. a^{-1} in this study, keeping in mind that they use local-specific bias correction and calibration. Furthermore, the positive measured annual mass balances in 2015 and 2016 are not simulated either in the simulations of the publication or in Kronenberg and others (2022). A master thesis at Humboldt-Universität, Berlin, supervised by both authors revealed the same: ERA5-L is not capable of reproducing the annual mass balance patterns of ABR with high agreement. In the case of NAI, the data quality is hard to assess. The second author participated in two field campaigns to NAI in 2011 and 2012. NAI is a very remote glacier without a permanent research station close by. The years 2006–2010 are the only ever reported values for NAI. Presumably, the few stake-based observations in the accumulation area probably do not account for refreezing over the vast accumulation area of NAI. This might explain why simulated mass balance is less negative than the observations from 2008–2010. The years 2006 and 2007 in turn are merely represented as a single observation over two years.

In Fig. S12 simulated and measured mass balance profiles of the five glaciers from which point mass-balance measurements exist are displayed. All single observations within the same 50-m band were averaged. From the simulation, the average of all GGPs that fall within the same 50-m band was taken. In general, the measured altitudinal $b_{clim,a}$ can be reproduced very well by the model. It should be noted that point measurements always have very site-specific properties that cannot always be reproduced by model simulations that provide areal averages depending on spatial resolution. A possible reason for the more positive mass balance in the accumulation area of BIC, UG1, and YAL could be refreezing, which is likely not included in the observations, since the increase in density of snow and firn would have to be measured between years to account for this positive mass-balance effect. For UG1, the authors know from their own field experience that no mass-balance observations are carried out in the steep headwalls of the accumulation areas where accumulation is typically very high. This is another reason why it is likely that observations underestimate accumulation in the highest areas to some extent. In the case of YAL the mismatch might be related to the very high scaling factor of annual *TP*.

Figure S16 and Fig. S17 show the daily energy- and mass-balance fluxes of KYS and NAI on 7 July 2007. With the increase of net shortwave radiation during the day, the surface heats up to 273.16 K and melt energy is generated. This is followed by refreezing of the percolation water within the snow layers and, with a time lag, a positive Q_G (i.e. through release of latent heat by refreezing). Energy is then released into the atmosphere through a negative R_N. The same pattern is perceivable in both cases. The day was chosen arbitrarily.

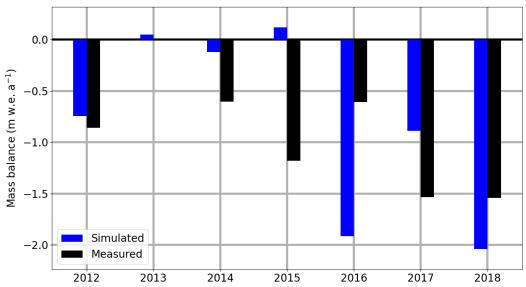

(a) Yala Glacier

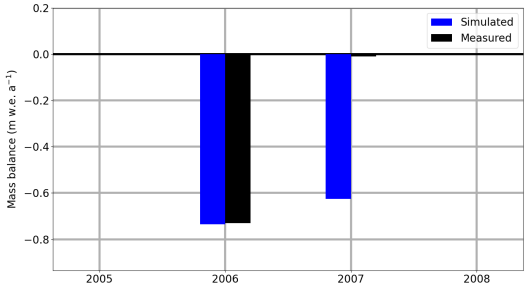

(b) Parlung No. 4 glacier

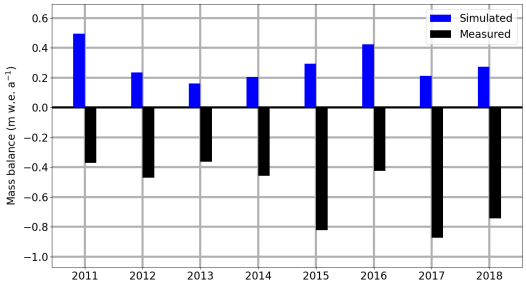

(c) Batysh Sook glacier

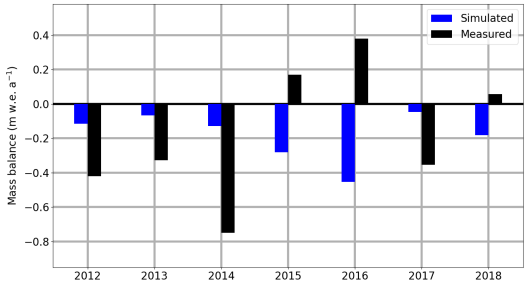

(d) Abramov glacier

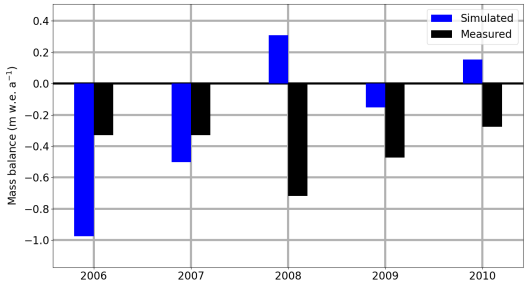

(e) Naimonayi glacier

Fig. S11. Comparison of the annual glacier-wide climatic mass balance with mass balance measurements published by the World Glacier Monitoring Service (WGMS, 2021).

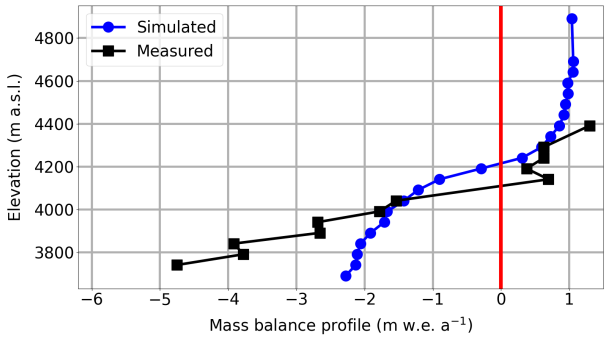

(a) Abramov glacier

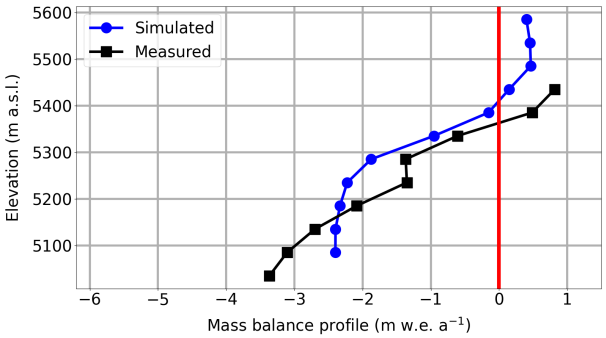

(b) Parlung No. 94 glacier

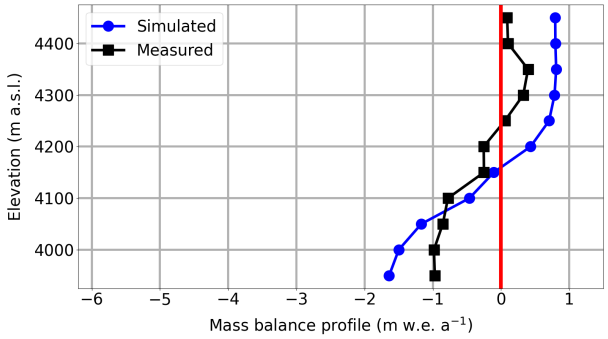

(c) Batysh Sook glacier

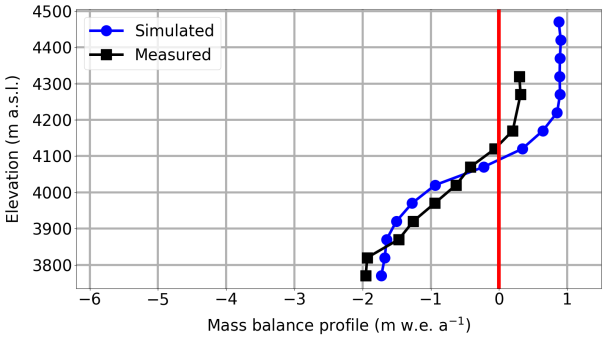

(d) Urumqi Glacier No. 1

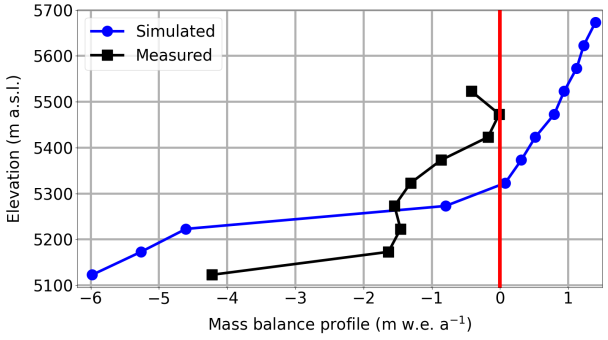

(e) Yala Glacier

Fig. S12. Comparison of simulated annual climatic mass balance profiles (mean mass-balance years 2001-2018) with measured mass balance profiles by World Glacier Monitoring Service (WGMS, 2021).

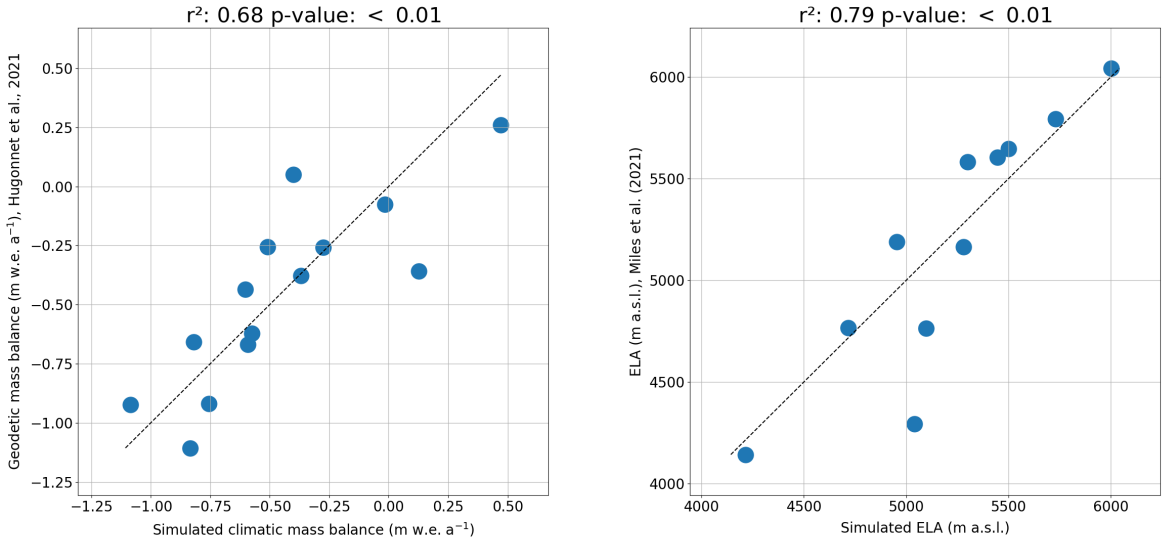

(a) Hugonnet and others (2021)

(b) Miles and others (2021)

Fig. S13. Scatterplot of glacier-wide cumulative climatic mass balance of the studied glaciers and the geodetic mass balance by Hugonnet and others (2021) and simulated equilibrium line altitude and the derived equilibrium line altitude by Miles and others (2021). A linear least-square regression model is used for the statistics.

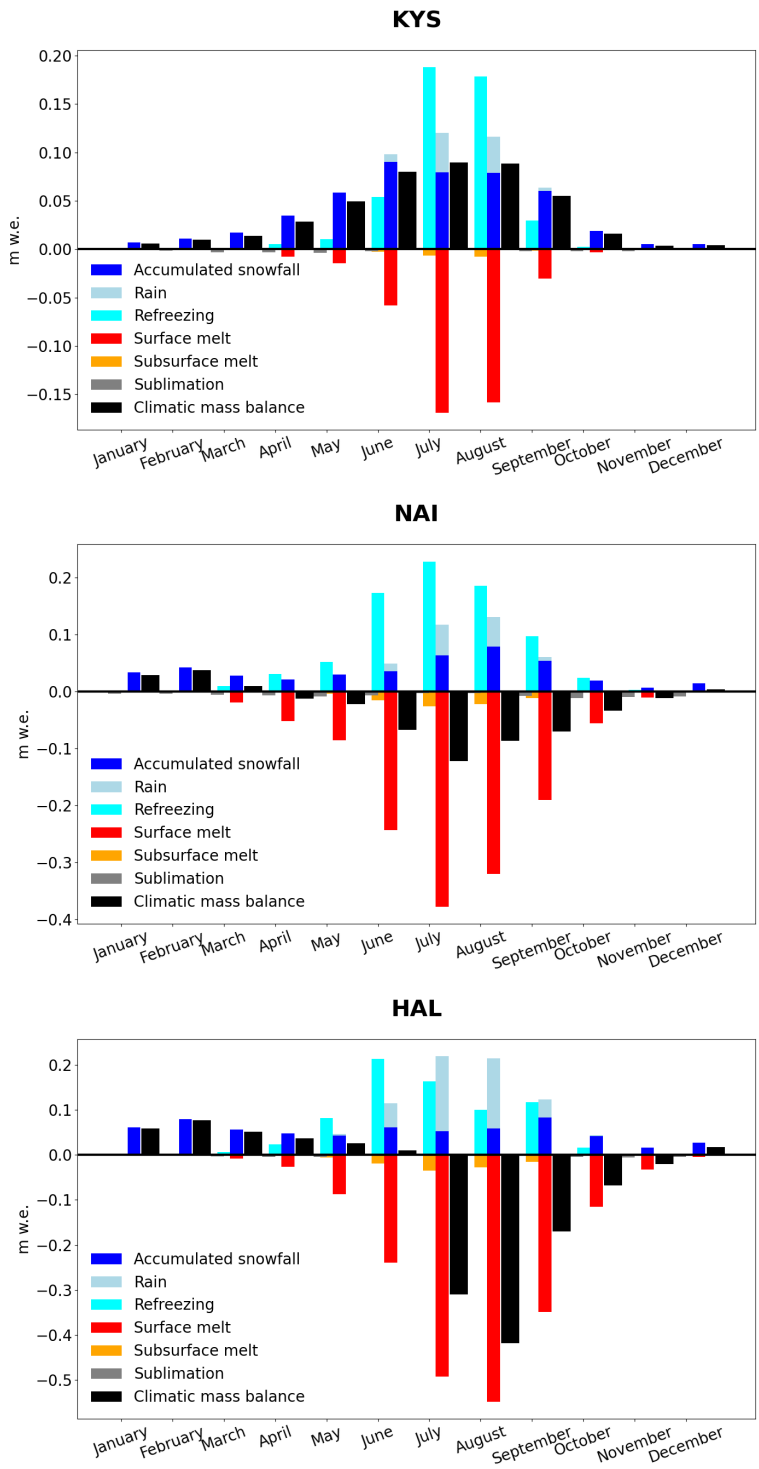

Fig. S14. The long-term (mass-balance year 2001–2018) mean monthly mass fluxes of Keli Yanghe source glacier (KYS), Naimonayi glacier (NAI), and Halji glacier (HAL).

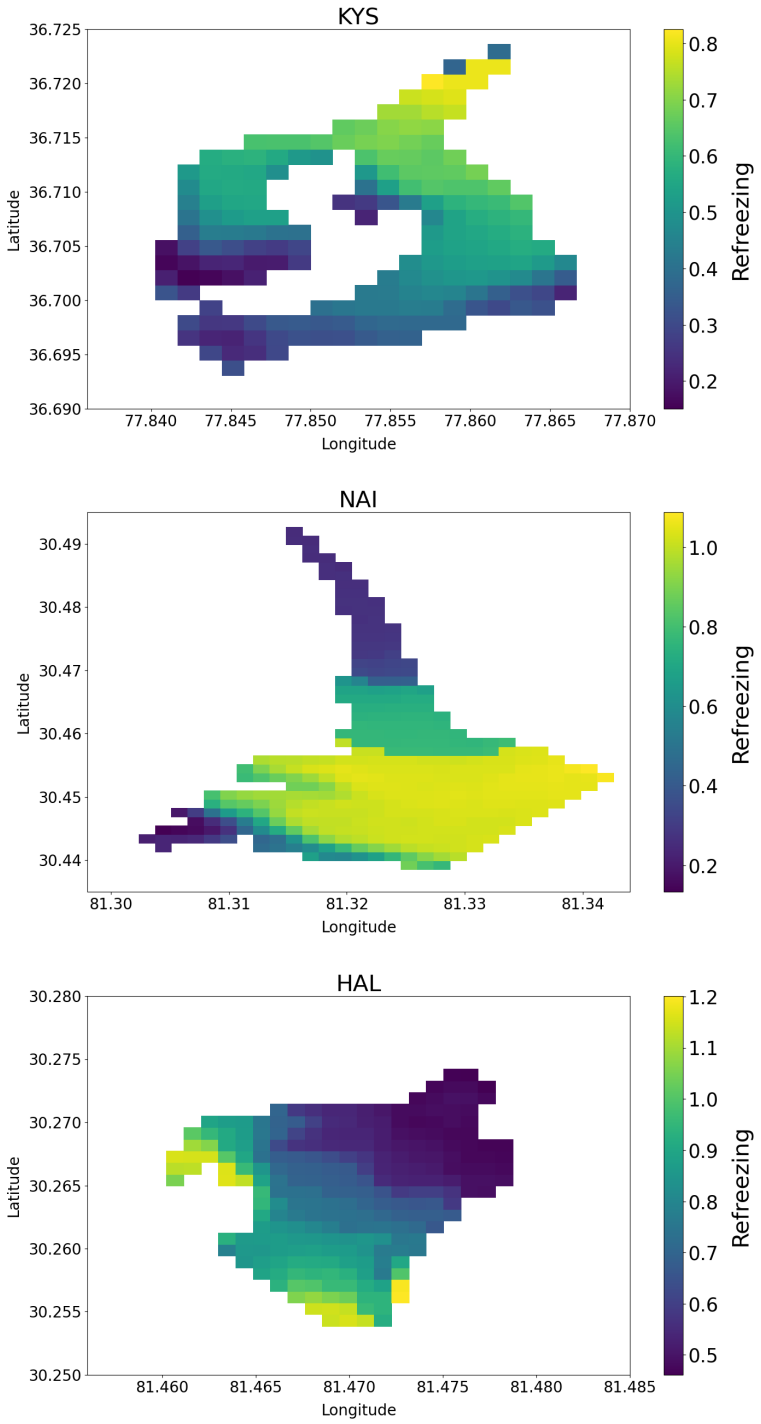

Fig. S15. Annual mean (mass-balance year 2001–2018) refreezing (m w.e. a^{-1}) of Keli Yanghe source glacier (KYS), Naimonayi glacier (NAI), and Halji glacier (HAL). KYS and HAL are northwest facing and NAI is north facing. Please note the different scaling of the colorbar.

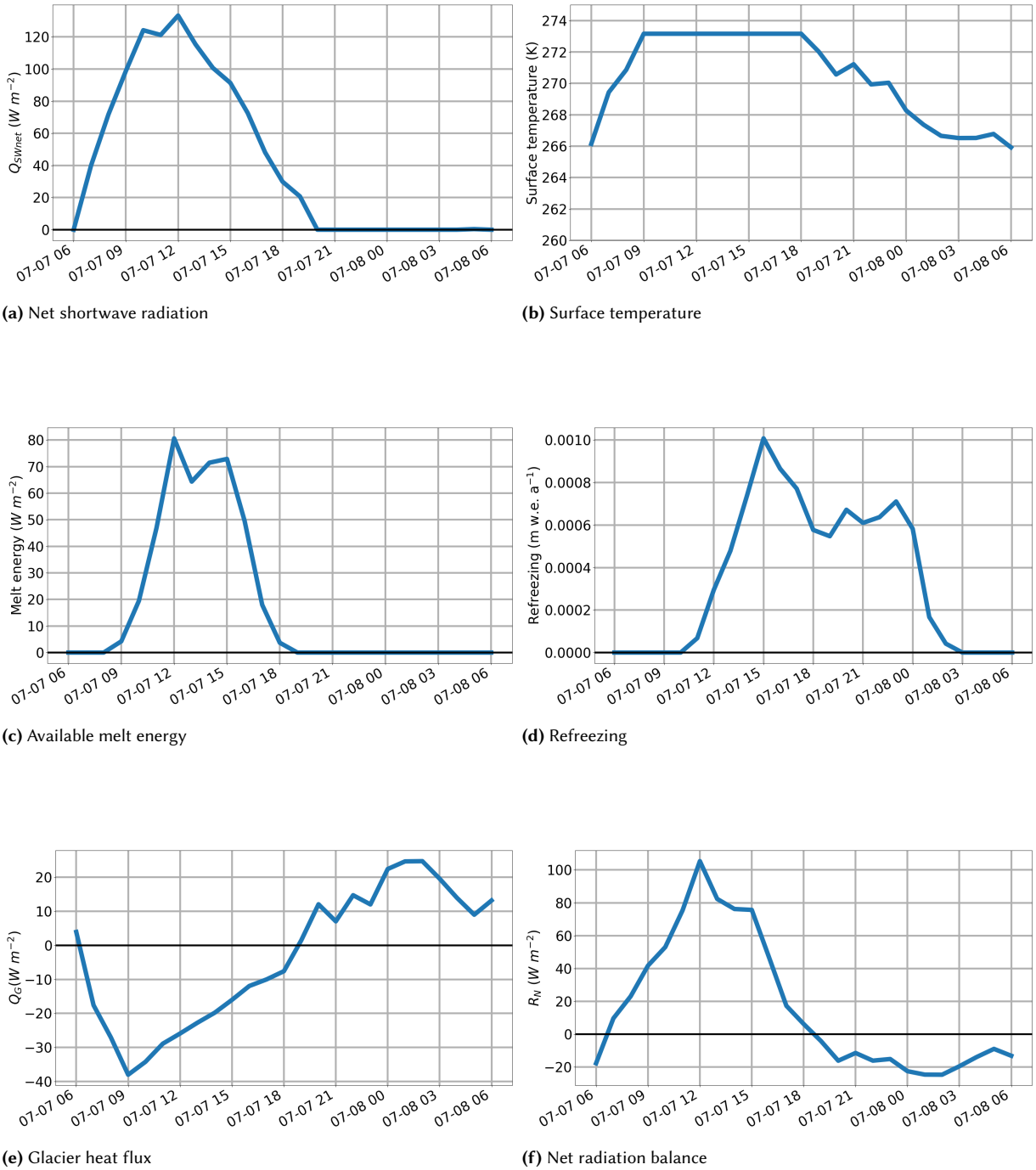

(a) Net shortwave radiation

(b) Surface temperature

(c) Available melt energy

(d) Refreezing

(e) Glacier heat flux

(f) Net radiation balance

Fig. S16. Energy and mass balance terms of one glacier grid point (36.717°N, 77.856°E) of Keli Yanghe source glacier (KYS), on 7 July 2007.

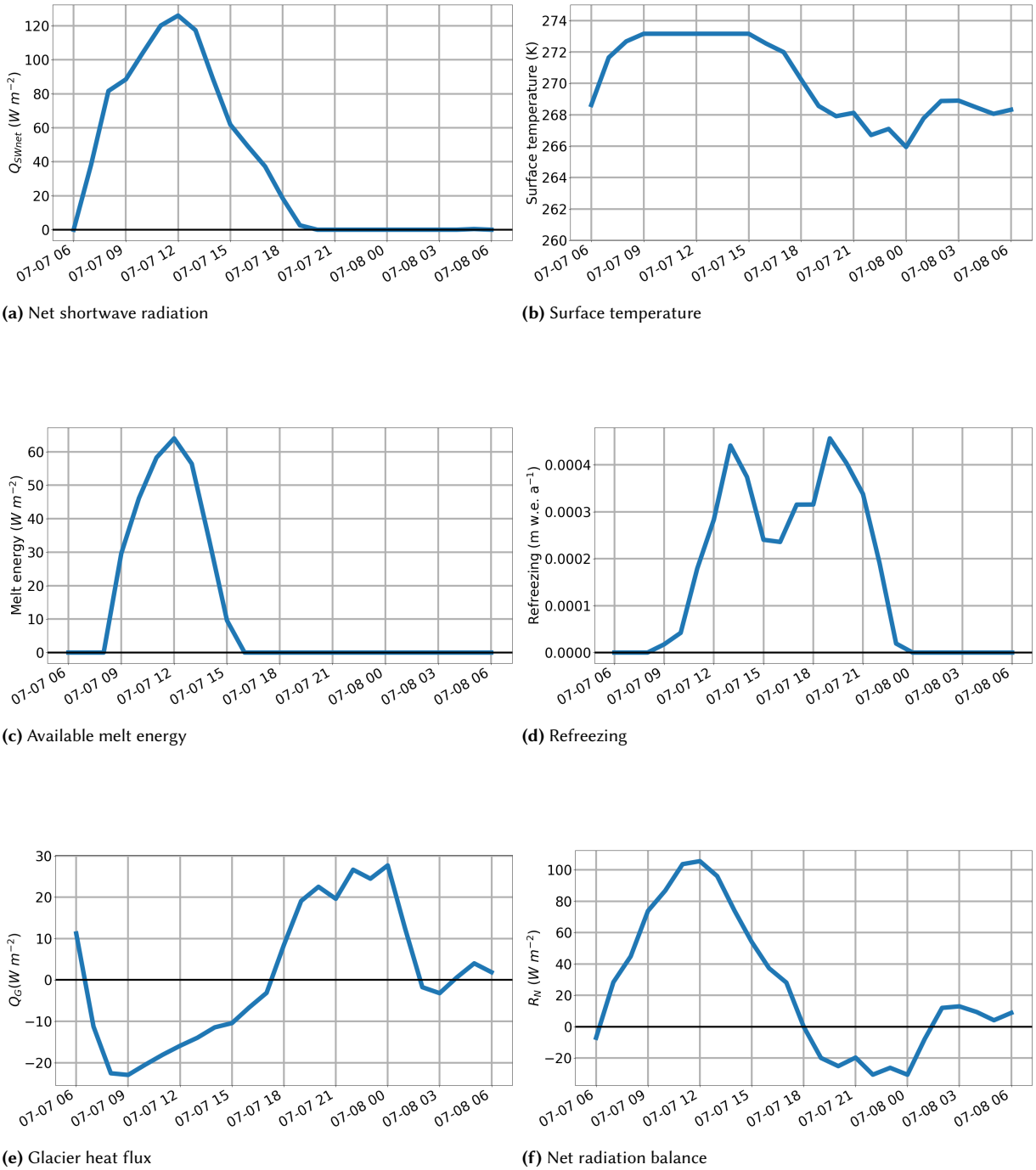

(a) Net shortwave radiation

(b) Surface temperature

(c) Available melt energy

(d) Refreezing

(e) Glacier heat flux

(f) Net radiation balance

Fig. S17. Energy and mass balance terms of one glacier grid point (30.44°N, 81.32°E) of Naimonayi glacier (NAI) on 7 July 2007.

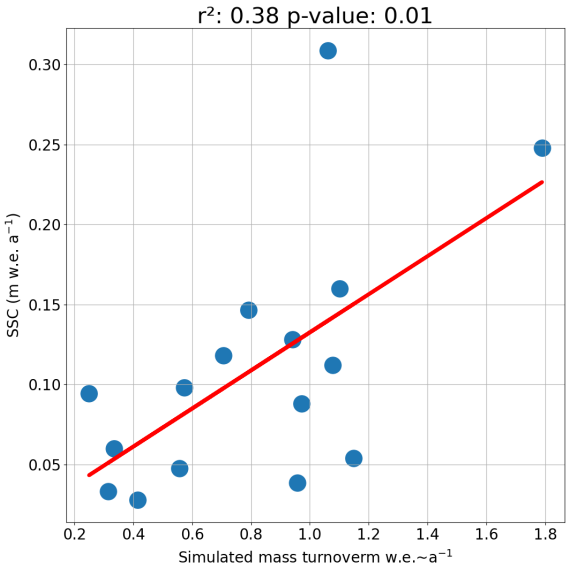

Fig. S18. Scatterplot of mean seasonal sensitivity characteristics SC_{sea} and mass turnover of the 16 studied glaciers. The mean SC_{sea} is calculated as the sum of the mean of the 12 *TP* SC_{sea} values and the absolute value of the mean of the 12 T_2 SC_{sea} values of each glacier.

REFERENCES

Azam MF, Ramanathan A, Wagnon P, Vincent C, Linda A, Berthier E, Sharma P, Mandal A, Angchuk T, Singh V and Pottakkal J (2016) Meteorological conditions, seasonal and annual mass balances of Chhota Shigri Glacier, western Himalaya, India. *Annals of Glaciology*, **57**(71), 328–338 (doi: 10.3189/2016AoG71A570)

Hugonnet R, McNabb R, Berthier E, Menounos B, Nuth C, Girod L, Farinotti D, Huss M, Dussaillant I, Brun F and Kääb A (2021) Accelerated global glacier mass loss in the early twenty-first century. *Nature*, **592**(7856), 726–731 (doi: 10.1038/s41586-021-03436-z)

Kronenberg M, van Pelt W, Machguth H, Fiddes J, Hoelzle M and Pertziger F (2022) Long-term firn and mass balance modelling for Abramov Glacier in the data-scarce Pamir Alay. *The Cryosphere*, **16**(12), 5001–5022 (doi: 10.5194/tc-16-5001-2022)

Miles E, McCarthy M, Dehecq A, Kneib M, Fugger S and Pellicciotti F (2021) Health and sustainability of glaciers in High Mountain Asia. *Nature Communications*, **12**(1), 2868 (doi: 10.1038/s41467-021-23073-4)

Oerlemans J and Reichert B (2000) Relating glacier mass balance to meteorological data by using a seasonal sensitivity characteristic. *Journal of Glaciology*, **46**(152), 1–6 (doi: 10.3189/172756500781833269)

Shean DE, Bhushan S, Montesano P, Rounce DR, Arendt A and Osmanoglu B (2020) A Systematic, Regional Assessment of High Mountain Asia Glacier Mass Balance. *Frontiers in Earth Science*, **7**, 363 (doi: 10.3389/feart.2019.00363)

Stigter EE, Litt M, Steiner JF, Bonekamp PNJ, Shea JM, Bierkens MFP and Immerzeel WW (2018) The Importance of Snow Sublimation on a Himalayan Glacier. *Frontiers in Earth Science*, **6**, 108 (doi: 10.3389/feart.2018.00108)

WGMS (2021) Fluctuations of Glaciers Database. World Glacier Monitoring Service, Zurich, Switzerland. (doi: 10.5904/wgms-fog-2021-05)

Zhu M, Yao T, Yang W, Xu B, Wu G and Wang X (2018) Differences in mass balance behavior for three glaciers from different climatic regions on the Tibetan Plateau. *Climate Dynamics*, **50**, 3457–3484 (doi: 10.1007/s00382-017-3817-4)